Article

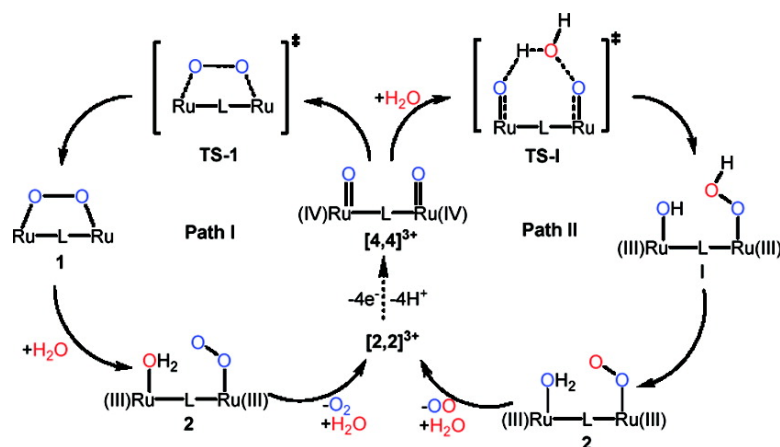# The Mechanism of Water Oxidation Catalysis Promoted by [tpyRu(IV)#O]L: A Computational Study

Xiaofan Yang, and Mu-Hyun Baik

More About This Article

Additional resources and features associated with this article are available within the HTML version:

- Supporting Information
- Access to high resolution figures
- Links to articles and content related to this article
- Copyright permission to reproduce figures and/or text from this article

View the Full Text HTML

The Mechanism of Water Oxidation Catalysis Promoted by [tpyRu(IV)=O]$_2$L^{3+}: A Computational Study

Xiaofan Yang and Mu-Hyun Baik*

Department of Chemistry, Indiana University, Bloomington, Indiana 47405, and Institut für Chemie, Technische Universität Berlin, D-10623 Berlin, Germany

Received May 7, 2008; E-mail: mbaik@indiana.edu

Abstract: The resting state of the recently reported water oxidation catalyst [tpyRu(II)−OH$_2$]$_2$L^{3+} (tpy = terpyridine; L = bipyridylpyrazolylic anion) (**[2,2]**$^{3+}$) must be activated by a series of proton-coupled oxidations in which four protons and four electrons are removed overall to afford the catalytically competent species [tpyRu(IV)=O]$_2$L^{3+} (**[4,4]**$^{3+}$). We have examined all of the plausible redox intermediates utilizing density functional theory coupled to a continuum solvation model. Our calculations reproduce well the first three redox potentials under pH = 1 conditions, and a reasonable correlation between theory and experiment is found for the fourth irreversible redox process that accompanies O$_2$ generation. The computed oxidation potentials to access **[5,4]**$^{4+}$ and **[5,5]**$^{5+}$, 1.875 and 2.032 V vs NHE, respectively, exclude the otherwise plausible possibilities of the catalytically active species having a higher oxidation state. **[4,4]**$^{3+}$ has an antiferromagnetically coupled ground state in which one ruthenium has two unpaired electrons antiparallel to those of the other ruthenium. As we found in our previous work, two radicaloid terminal oxygen moieties with different spin orientations that are induced by spin polarization from the electron-deficient Ru(IV) centers are found. Two mechanistic scenarios are relevant and interesting for the key O−O bond formation event: intramolecular oxo−oxo coupling and coupling between one terminal oxo and the oxygen atom of the incoming water substrate. The intramolecular oxo−oxo coupling is facile, with a low barrier of 13.9 kcal mol^{-1}, yielding a peroxo intermediate. The necessary subsequent addition of water in an associative substitution mechanism to cleave one of the Ru−peroxo bonds, however, is found to be impractical at room temperature, with a barrier of $\Delta G^{\ddagger} = 30.9$ kcal mol^{-1}. Thus, while plausible, the intramolecular oxo−oxo coupling is unproductive for generating molecular dioxygen. The intermolecular O−O coupling is associated with a high barrier ($\Delta G^{\ddagger} = 40.2$ kcal mol^{-1}) and requires the assistance of an additional proton, which lowers the barrier dramatically to 24.5 kcal mol^{-1}.

Introduction

The imminent need to develop a renewable and sustainable source for energy that provides an alternative to fossil fuels has recently inspired much research, with solar energy likely being the only long-term solution.[1] Inspired by the photosynthesis performed by green plants, one can envision a conceptual model of a "solar fuel cell",[1] as shown in Scheme 1. The immediate and primary products can be the water electrolysis products O$_2$ and H$_2$, which may be utilized as energy carriers.[2,3] A more futuristic vision involves using the electrons harvested from water oxidation to catalyze CO$_2$ activation in an artificial photosynthetic framework, producing hydrocarbons that can ultimately be used as substitute fossil fuels. The most challenging component of this visionary model system is the thermodynamically demanding anodic reaction, which supplies electrons by oxidizing water. In nature, green plants utilize a Mn$_4$ cluster found in the oxygen-evolving complex (OEC) to catalyze water oxidation (Scheme 2), generating free O$_2$ and harvesting

electrons for the subsequent reduction of CO$_2$ to sugars.[4,5] To make use of solar energy on the basis of the above model, we must understand how to promote and control water oxidation catalysis. Unfortunately, the complex protein environment[6,7] surrounding the Mn$_4$ core creates serious difficulties in accurately detecting and understanding how nature accomplishes this difficult task under ambient conditions.[4,8,9] In the past few decades, a handful of inorganic complexes[10−25] have been

(1) Lewis, N. S.; Nocera, D. G. *Proc. Natl. Acad. Sci. U.S.A.* **2006**, *103*, 15729−15735.
(2) Dreier, T.; Wagner, U. *BWK: Brennst., Wärme, Kraft* **2000**, *52*, 41−46.
(3) Dreier, T.; Wagner, U. *BWK* **2001**, *53*, 47−54.
(4) Yachandra, V. K.; Sauer, K.; Klein, M. P. *Chem. Rev.* **1996**, *96*, 2927−2950.
(5) Manchanda, R.; Brudvig, G. W.; Crabtree, R. H. *Coord. Chem. Rev.* **1995**, *144*, 1−38.
(6) Barber, J. *Inorg. Chem.* **2008**, *47*, 1700−1710.
(7) Ferreira, K. N.; Iverson, T. M.; Maghlaoui, K.; Barber, J.; Iwata, S. *Science* **2004**, *303*, 1831−1838.
(8) Yano, J.; Yachandra, V. K. *Inorg. Chem.* **2008**, *47*, 1711−1726.
(9) Yeagle, G. J.; Gilchrist, M. L.; McCarrick, R. M.; Britt, R. D. *Inorg. Chem.* **2008**, *47*, 1803−1814.
(10) Gilbert, J. A.; Eggleston, D. S.; Murphy, W. R.; Geselowitz, D. A.; Gersten, S. W.; Hodgson, D. J.; Meyer, T. J. *J. Am. Chem. Soc.* **1985**, *107*, 3855−3864.
(11) Sens, C.; Romero, I.; Rodriguez, M.; Llobet, A.; Parella, T.; Benet-Buchholz, J. *J. Am. Chem. Soc.* **2004**, *126*, 7798−7799.
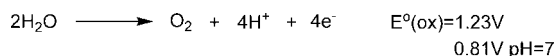(12) Naruta, Y.; Sasayama, M.; Sasaki, T. *Angew. Chem., Int. Ed. Engl.* **1994**, *33*, 1839−1841.
(13) Poulsen, A. K.; Rompel, A.; McKenzie, C. J. *Angew. Chem., Int. Ed.* **2005**, *44*, 6916−6920.

Scheme 1

Scheme 2

$$2H_2O \longrightarrow O_2 + 4H^+ + 4e^- \qquad E^o(ox) = 1.23V$$
$$0.81V \ pH = 7$$
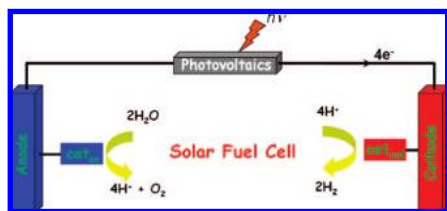
developed to mimic the reactivity of the Mn_4 component in the OEC. Beyond the most popular bimetallic catalysts having two M=O moieties (M = Ru or Mn) at the active states, e.g., the "blue dimer"[10] and the dimanganese complex of Brudvig and Crabtree,[14] there are also catalysts with single metal centers[26,27] or a tetraruthenium core[28,29] sharing similar structural features with the active Mn_4 site in the OEC. Unfortunately, our current understanding of the mechanistic features critical for water oxidation catalysis is poor at best, and there is no strategy available for a systematic improvement of these catalysts. Our previous studies[30,31] on the blue dimer demonstrated that density functional theory (DFT) is sufficiently accurate to provide useful mechanistic insights at the atomistic level when the results are evaluated critically and carefully. While they are far from being quantitatively reliable and leave many important questions, e.g., spectroscopic signature, unanswered, these calculations can offer intuitively comprehensible concepts of what may be driving the water catalysis.

For the bimetallic catalysts, we proposed that terminal oxo groups formed by oxidizing the metals to sufficiently high oxidation states and removing protons from the original aqua ligands are the active sites of the water splitting reaction.[30,31] Among the many mechanistic speculations on the key O−O bond formation process required as part of the water oxidation
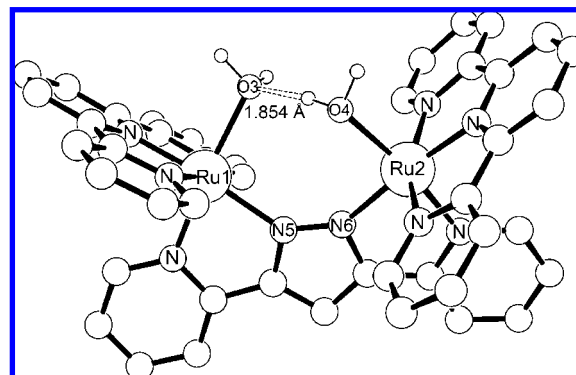
(14) Limburg, J.; Vrettos, J. S.; Liable-Sands, L. M.; Rheingold, A. L.; Crabtree, R. H.; Brudvig, G. W. *Science* **1999**, *283*, 1524–1527.
(15) Zong, R.; Thummel, R. P. *J. Am. Chem. Soc.* **2005**, *127*, 12802–12803.
(16) Eisenberg, R.; Gray, H. B. *Inorg. Chem.* **2008**, *47*, 1697–1699.
(17) Liu, F.; Concepcion, J. J.; Jurss, J. W.; Cardolaccia, T.; Templeton, J. L.; Meyer, T. J. *Inorg. Chem.* **2008**, *47*, 1727–1752.
(18) Hurst, J. K.; Cape, J. L.; Clark, A. E.; Das, S.; Qin, C. *Inorg. Chem.* **2008**, *47*, 1753–1764.
(19) Pecoraro, V. L.; Hsieh, W. Y. *Inorg. Chem.* **2008**, *47*, 1765–1778.
(20) Muckerman, J. T.; Polyansky, D. E.; Wada, T.; Tanaka, K.; Fujita, E. *Inorg. Chem.* **2008**, *47*, 1787–1802.
(21) Tagore, R.; Crabtree, R. H.; Brudvig, G. W. *Inorg. Chem.* **2008**, *47*, 1815–1823.
(22) Deng, Z.; Tseng, H.-W.; Zong, R.; Wang, D.; Thummel, R. *Inorg. Chem.* **2008**, *47*, 1835–1848.
(23) Betley, T. A.; Wu, Q.; Voorhis, T. V.; Nocera, D. G. *Inorg. Chem.* **2008**, *47*, 1849–1861.
(24) Siegbahn, P. E. *Inorg. Chem.* **2008**, *47*, 1779–1786.
(25) Romero, I.; Rodríguez, M.; Sens, C.; Mola, J.; Rao Kollipara, M. R.; Francàs, L.; Mas-Marza, E.; Escriche, L.; Llobet, A. *Inorg. Chem.* **2008**, *47*, 1824–1834.
(26) Ledney, M.; Dutta, P. K. *J. Am. Chem. Soc.* **1995**, *117*, 7687–7695.
(27) McDaniel, N. D.; Coughlin, F. J.; Tinker, L. L.; Bernhard, S. *J. Am. Chem. Soc.* **2008**, *130*, 210–217.
(28) Geletii, Y. V.; Botar, B.; Kögerler, P.; Hillesheim, D. A.; Musaev, D. G.; Hill, C. L. *Angew. Chem., Int. Ed.* **2008**, *47*, 3896–3899.
(29) Sartorel, A.; Carraro, M.; Scorrano, G.; Zorzi, R. D.; Geremia, S.; McDaniel, N. D.; Bernhard, S.; Bonchio, M. *J. Am. Chem. Soc.* **2008**, *130*, 5006–5007.
(30) Yang, X.; Baik, M.-H. *J. Am. Chem. Soc.* **2006**, *128*, 7476–7485.
(31) Yang, X.; Baik, M.-H. *J. Am. Chem. Soc.* **2004**, *126*, 13222–13223.

Figure 1. Optimized structure of $[tpyRu^{II}OH_2]_2L^{3+}$ **[2,2]$^{3+}$** (tpy = terpyridine, L = bipyridylpyrazolylic anion).

Scheme 3
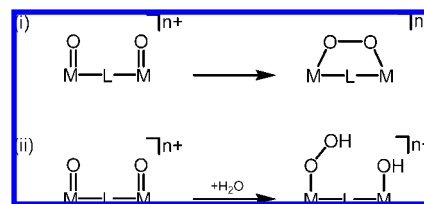
reaction,[32] two are most attractive (Scheme 3): (i) Direct coupling between the two terminal oxo groups affords a bimetallic peroxo compound with each metal reduced by one electron. The resulting intermediate undergoes reductive elimination coupled with water addition to release free molecular oxygen, closing the overall four-electron transfer cycle and regenerating the catalyst resting state. (ii) Coupling between the terminal oxo and water oxygen atom provides a hydroxo/hydroperoxo intermediate, which is the precursor to O_2 release. The second route was identified to be operative for the blue dimer both experimentally[33] and computationally[31] in previous studies. The first route, which should in principle be more favorable entropically for the key O−O bond formation process, was not supported by experimental or theoretical studies. A diruthenium complex recently reported by Llobet,[11] denoted **[2,2]$^{3+}$** (Figure 1), attracted our attention as a candidate for the intramolecular O−O bond formation route because (i) the two terminal oxygen atoms are conformationally locked by the rigid bridging bipyridylpyrazolylic ligand in a facial manner, as opposed to the flexibility introduced by the Ru−O−Ru bridging system in the blue dimer, and (ii) the catalytic ability of **[2,2]$^{3+}$** is very comparable to that of the blue dimer under acidic conditions. In this work, we are interested in both understanding the electronic properties of the new catalyst and discovering in detail how it catalyzes the water oxidation reaction.

Computational Details

All of the calculations were carried out using DFT as implemented in the Jaguar 5.5 suite[34] of *ab initio* quantum chemistry programs. Geometry optimizations were performed with the B3LYP[35−39] functional using the 6-31G** basis set. Ruthenium

(32) Ruettinger, W.; Dismukes, G. C. *Chem. Rev.* **1997**, *97*, 1–24.
(33) Yamada, H.; Siems, W. F.; Koike, T.; Hurst, J. K. *J. Am. Chem. Soc.* **2004**, *126*, 9786–9795.
(34) Jaguar, version 5.5; Schrödinger, Inc.: Portland, OR, 2003.
(35) Becke, A. D. *Phys. Rev. A* **1988**, *38*, 3098–3100.
(36) Becke, A. D. *J. Chem. Phys.* **1993**, *98*, 5648–5652.
(37) Lee, C. T.; Yang, W. T.; Parr, R. G. *Phys. Rev. B* **1988**, *37*, 785–789.
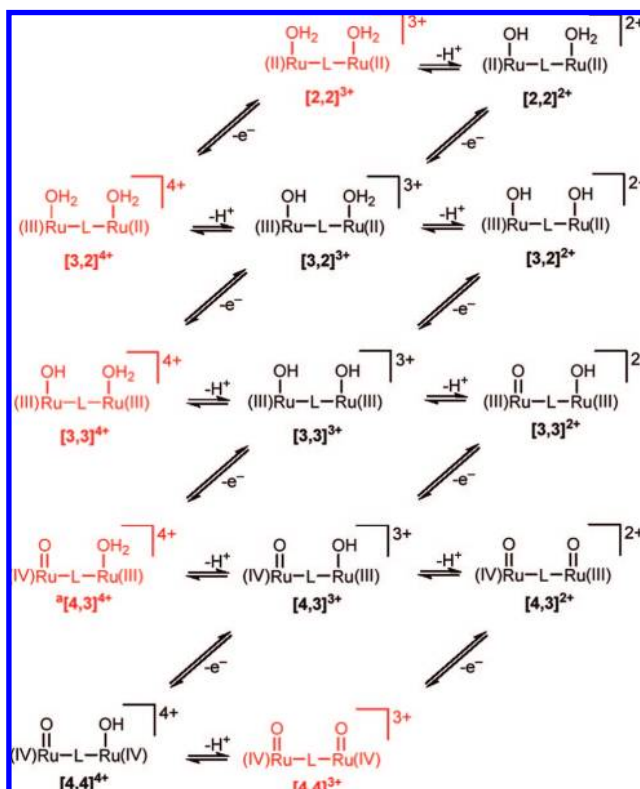
was represented with the Los Alamos LACVP basis[40,41] that includes relativistic effective core potentials. The energies of the optimized structures were reevaluated by additional single-point calculations at each optimized geometry using Dunning's correlation-consistent triple-ζ basis set cc-pVTZ(-f),[42] which includes a double set of polarization functions. For ruthenium, we used a modified version of LACVP, designated as LACV3P, in which the exponents were decontracted to match the effective core potential with the triple-ζ quality basis. Vibrational frequency calculations based on analytical second derivatives at the B3LYP/6-31G** (LACVP) level of theory were carried out on smaller models to derive the zero-point vibrational energy (ZPE) and entropy corrections at room temperature utilizing unscaled frequencies. It should be noted that by entropy here we refer specifically to the vibrational/rotational/translational entropy of the solute(s); the entropy of the solvent is implicitly included in the dielectric continuum model. The molecules used for vibrational frequency calculations were derived from the corresponding fully optimized structures by replacing each terpyridine group with three ammonia ligands. In a few cases, we also carried out vibrational frequency calculations on the full models, either to compare with the redox potentials calculated using truncated models (Table S5 in the Supporting Information) or to verify the validity of several important transition state (TS) structures, i.e., **TS-2H$_T$** and **TS-IH$_{AF}$**. Because of the extremely high computational cost of these calculations, they were only done for selected species. Solvation energies were evaluated by a self-consistent reaction field (SCRF)[43−45] approach based on accurate numerical solutions of the Poisson−Boltzmann equation.[46] These calculations were carried out at the optimized gas-phase geometries, employing a dielectric constant (ϵ) value of 80.37 (water). As is the case for all continuum models, the solvation energies are subject to empirical parametrization of the atomic radii that are used to generate the solute surface. We employed the standard set[46] of optimized radii in Jaguar for H (1.150 Å), C (1.900 Å), N (1.600 Å), and O (1.600 Å) and 1.481 Å for Ru. All of the calculations made use of the unrestricted spin formalism. Antiferromagnetically coupled states were modeled, where appropriate, using the broken-symmetry (BS) orbital approach.[47,48]

Accurate computation of redox potentials in the solution phase is challenging. In previous work, we established that DFT calculations with a triple-ζ basis in combination with a continuum solvation model can reproduce experimental redox potentials remarkably well. We found typical errors to be on the order of 150 mV with our previously published protocol.[49] For computations involving proton-coupled redox reactions, it is necessary to account for the energy of a proton in solution. We used the following expression to compute $G(\text{H}^+)$, the free energy of a proton in solution:

$$G(\text{H}^+) = H^{gas}(\text{H}^+) - TS + \tfrac{5}{2}RT + G^{solv}(\text{H}^+) \quad (1)$$

where $H^{gas}(\text{H}^+)$, the gas-phase electronic energy, is zero by definition; R is the gas constant; T is 298.15 K; S is the translational

(38) Slater, J. C. *Quantum Theory of Molecules and Solids, Vol. 4: The Self-Consistent Field for Molecules and Solids*; McGraw-Hill: New York, 1974.
(39) Vosko, S. H.; Wilk, L.; Nusair, M. *Can. J. Phys.* **1980**, *58*, 1200–1211.
(40) Hay, P. J.; Wadt, W. R. *J. Chem. Phys.* **1985**, *82*, 270–283.
(41) Hay, P. J.; Wadt, W. R. *J. Chem. Phys.* **1985**, *82*, 299–310.
(42) Dunning, T. H. *J. Chem. Phys.* **1989**, *90*, 1007–1023.
(43) Edinger, S. R.; Cortis, C.; Shenkin, P. S.; Friesner, R. A. *J. Phys. Chem. B* **1997**, *101*, 1190–1197.
(44) Cortis, C. M.; Friesner, R. A. *J. Comput. Chem.* **1997**, *18*, 1570–1590.
(45) Cortis, C. M.; Friesner, R. A. *J. Comput. Chem.* **1997**, *18*, 1591–1608.
(46) Rashin, A. A.; Honig, B. *J. Phys. Chem.* **1985**, *89*, 5588–5593.
(47) Noodleman, L.; Lovell, T.; Han, W.-G.; Li, J.; Himo, F. *Chem. Rev.* **2004**, *104*, 459–508.
(48) Noodleman, L. *J. Chem. Phys.* **1981**, *74*, 5737–5743.
(49) Baik, M.-H.; Friesner, R. A. *J. Phys. Chem. A* **2002**, *106*, 7407–7415.

Scheme 4

entropy of a free hydrogen atom calculated using the Sackur−Tetrode equation (26.04 eu); $\tfrac{5}{2}RT$ is the thermal correction, which amounts to 0.064 eV at 298.15 K; and $G^{solv}(\text{H}^+)$ is the free energy of solvation of a proton (-262.23 kcal mol^{-1}).[50] At 298.15 K, eq 1 yields $G(\text{H}^+) = -11.644$ eV. Since experimental redox potentials are measured at pH 1, our computed standard redox potentials were adjusted to the experimental pH conditions using the Nernst equation:

$$E_{1/2}(\text{calcd})_{pH} = E_{1/2}(\text{calcd}) - \frac{RT\ln(10)}{n_e} \times n_{\text{H}^+} \times \text{pH} \quad (2)$$

where n_e and n_{H^+} are the numbers of electrons and protons, respectively, involved in the redox reaction. The value of RT is computed to be 0.0257 V at 298.15 K; thus, according to eq 2, $\sim$59 mV should be subtracted from the computed standard redox potentials when one proton is involved in the redox reaction at pH 1.

Results and Discussion

Redox Properties of Plausible Oxidation States. Compound **[2,2]³⁺** loses in total four electrons and four protons when it is transformed to the catalytically active complex [tpyRu-(IV)=O]₂L³⁺ **[4,4]³⁺**, as suggested by the Pourbaix diagram previously reported by Llobet.[11] Scheme 4 shows a selection of plausible redox intermediates that we have considered and carefully examined. The most abundant redox species for each oxidation state at pH 1 according to our calculated energies is shown in red. The computed pK_{a1} values are in accord with the experimental values within the standard range of error (Table 1).[51,52] The calculated pK_{a2} values are consistently shifted to

(50) Tawa, G. J.; Topol, I. A.; Burt, S. K.; Caldwell, R. A.; Rashin, A. A. *J. Chem. Phys.* **1998**, *109*, 4852–4863.
(51) Richardson, W. H.; Peng, C.; Bashford, D.; Noodleman, L.; Case, D. A. *Int. J. Quantum Chem.* **1997**, *61*, 207–217.

Table 1. Calculated pK_a Values for **[2,2]**, **[3,2]**, **[3,3]**, **[4,3]**, and **[4,4]** Ions (Values in Parentheses Are Experimental Values from Ref 11)

	pK_{a1}		pK_{a2}	
[2,2]$^{3+}$	7.5 (6.6)	**[2,2]**$^{2+}$		
[3,2]$^{4+}$	−0.1 (2.0)	**[3,2]**$^{3+}$	23.5 (10)	**[3,2]**$^{2+}$
[3,3]$^{4+}$	5.9	**[3,3]**$^{3+}$	24.7	**[3,3]**$^{2+}$
ᵃ[4,3]$^{4+}$	2.9	**[4,3]**$^{3+}$	33.9	**[4,3]**$^{2+}$
[4,4]$^{4+}$	−2.1	**[4,4]**$^{3+}$		

unrealistically higher values, which implies that either the states with +2 charge exist as more complex forms in the solution phase, for which we did not account, or the continuum solvation model fails to overcome the systematic error for this particular charge state.[53] Since none of the ions with +2 charge plays a significant role in the catalytic cycle under realistic experimental conditions, i.e., pH 1, we will not address or use these nonrealistic pK_{a2} values any further in this study. Structural parameters and Mulliken spin densities of the marked redox intermediates are summarized in Figures 1 and 2 and Tables 2 and 3. For the most important, highlighted redox species, an intramolecular hydrogen bond persists to higher oxidation states, with the exception of the **[4,4]**$^{3+}$ ion, which displays two terminal radicaloid oxyl groups similar to what we observed in the highest oxidation state of the blue dimer in our previous work.[30] Ideally, the Mulliken spin densities of the two rutheniums in **[4,4]**$^{3+}$, where each ruthenium has two unpaired electrons that couple antiferromagnetically to the other, should be close to 2.[54] The relatively small value of 0.9 arises from the neighboring electron-rich terminal oxo groups, whose electrons are largely polarized to compensate for the highly electron-deficient Ru(IV). Formally, the electronic structure of **[4,4]**$^{3+}$ can be envisioned as being closer to its resonance form displaying two radicaloid oxyl and antiferromagnetically coupled Ru(III) centers. This electronic feature is reminiscent of what we identified to be critical for the catalytically competent form of the blue dimer.[30] A more detailed molecular orbital characterization is presented in the Supporting Information. Following the single-electron transfer that transforms **[2,2]**$^{3+}$ into **[3,2]**$^{4+}$, there are two sequential proton-coupled electron-transfer (PCET) steps, which give rise to an unusually structured redox intermediate, denoted **ᵃ[4,3]**$^{4+}$, with two asymmetric subunits: Ru(IV)=O and Ru(III)−OH₂. The existence of an analogous diruthenium complex with oxo/aqua ligands but different oxidation states, formulated as [O=Ru(V)−O−Ru(III)−OH₂]$^{4+}$, was proposed by Meyer and co-workers in previous studies.[17,55,56] Our calculations indicate that the intrinsic preference of **ᵃ[4,3]**$^{4+}$ over **[4,3]**$^{4+}$ relies heavily on the electronic portion by as much as 12.9 kcal/mol, whereas ZPE, entropy, and solvation corrections contribute a small amount to afford a total free energy difference of 11.4 kcal/mol. A rationale for the formation of **ᵃ[4,3]**$^{4+}$ emerges at the electronic level if weak coupling between the two ruthenium centers in its redox precursor **[3,3]**$^{4+}$ is assumed. When the two subunits are exposed to nearly identical environments, the Ru(III)−OH subunit in **[3,3]**$^{4+}$ should be more reducing, in principle, than the Ru(III)−OH₂

subunit because of its higher frontier orbital energy induced by the stronger electrostatic field of OH⁻ versus OH₂. Therefore, it is plausible that the second PCET step occurs only on the individual Ru(III)−OH subunit of **[3,3]**$^{4+}$ to afford **ᵃ[4,3]**$^{4+}$. This assignment is further supported by redox potential calculations (Table 5 and Table S5 in the Supporting Information) that give a potential of 1.016 V compared to the experimentally observed 0.840 V. A notably higher potential of 1.510 V is computed when the involvement of **[4,3]**$^{4+}$ is assumed. To verify the plausibility of the antiferromagnetic (AF) coupling, we have probed all of the plausible spin states at oxidation levels of both **[3,3]** and **[4,4]**. Consistent with our previous conclusion from the blue dimer study,[31] if diamagnetism is assumed for the **[3,3]** and **[4,4]** ions, the weakly coupled AF states are significantly energetically favored over the closed-shell singlet (S) state (Table 4). Among all of the electronic structures we have sampled at the **[3,3]** and **[4,4]** oxidation states, AF states are identified to be the ground states within the standard DFT error,[58−60] with the notable exception of **[3,3]**$^{2+}$. The slightly reversed energy ordering between the AF and quintet (Q) states of the **[4,4]**$^{3+}$ ion is likely due to the intrinsic preference of hybrid DFT functionals for high-spin states.[61,62] Given the small energy difference (<1 kcal mol⁻¹) and the lack of experimental support for a paramagnetic intermediate in analogous systems, we move forward assuming the AF state to be the ground state of the **[4,4]**$^{3+}$ ion.

In our previous work,[49] a reasonably reliable protocol was developed for computing the redox potentials of species including transition metals. The same methodology has proven to succeed in reproducing the redox potentials of the blue dimer in various oxidation states[31] as well as in modeling its potential-inverted two-electron redox chemistry.[57] **[2,2]**$^{3+}$ was previously reported to undergo three reversible redox processes and an irreversible one accompanying O₂ formation at pH 1. Table 5 summarizes the calculated redox potentials and the corresponding experimental values. The calculated results reach a reasonable agreement for the first three reversible redox processes, but some discrepancy exists for the fourth redox process (row 5 in Table 5). While the disagreement of 304 mV between theory and experiment is unsettling, we note that the measurement of this potential was extremely difficult because of the irreversibility of this redox process and the intrinsic challenges of redox potential measurements at the highest redox states in general. We observed similar disagreements in the case of the blue dimer, where our calculation showed a deviation of ∼250 mV for the fourth irreversible electron-transfer process. In regard to the possibility of compounds in higher oxidation states than **[4,4]**$^{3+}$ catalyzing the water oxidation reaction, which is also plausible given the excess of oxidants typically used in these experiments and the fact that the voltammetric responses were very broad, the redox potentials computed for forming **[5,4]**$^{4+}$ and **[5,5]**$^{5+}$ from **[4,4]**$^{3+}$ are 1.875 and 2.032 V vs. NHE, respectively. These are difficult to impossible to access with Ce(IV) as the oxidant,

(52) Schmidt am Busch, M.; Knapp, E.-W. *ChemPhysChem* **2004**, *5*, 1513–1522.

(53) Cramer, C. J.; Truhlar, D. G. *Chem. Rev.* **1999**, *99*, 2161–2200.

(54) Mulliken, R. S. *J. Chem. Phys.* **1955**, *23*, 1833–1840.

(55) Binstead, R. A.; Chronister, C. W.; Ni, J. F.; Hartshorn, C. M.; Meyer, T. J. *J. Am. Chem. Soc.* **2000**, *122*, 8464–8473.

(56) Bartolotti, L. J.; Pedersen, L. G.; Meyer, T. J. *Int. J. Quantum Chem.* **2001**, *83*, 143–149.

(57) Yang, X.; Lord, R. L.; Baik, M.-H. unpublished results.

(58) Curtiss, L. A.; Raghavachari, K.; Redfern, P. C.; Pople, J. A. *J. Chem. Phys.* **1997**, *106*, 1063–1079.

(59) Curtiss, L. A.; Redfern, P. C.; Raghavachari, K.; Pople, J. A. *J. Chem. Phys.* **1998**, *109*, 42–55.

(60) Russo, T. V.; Martin, R. L.; Hay, P. J. *J. Chem. Phys.* **1994**, *101*, 7729–7737.

(61) Reiher, M.; Salomon, O.; Hess, B. A. *Theor. Chem. Acc.* **2001**, *107*, 48–55.

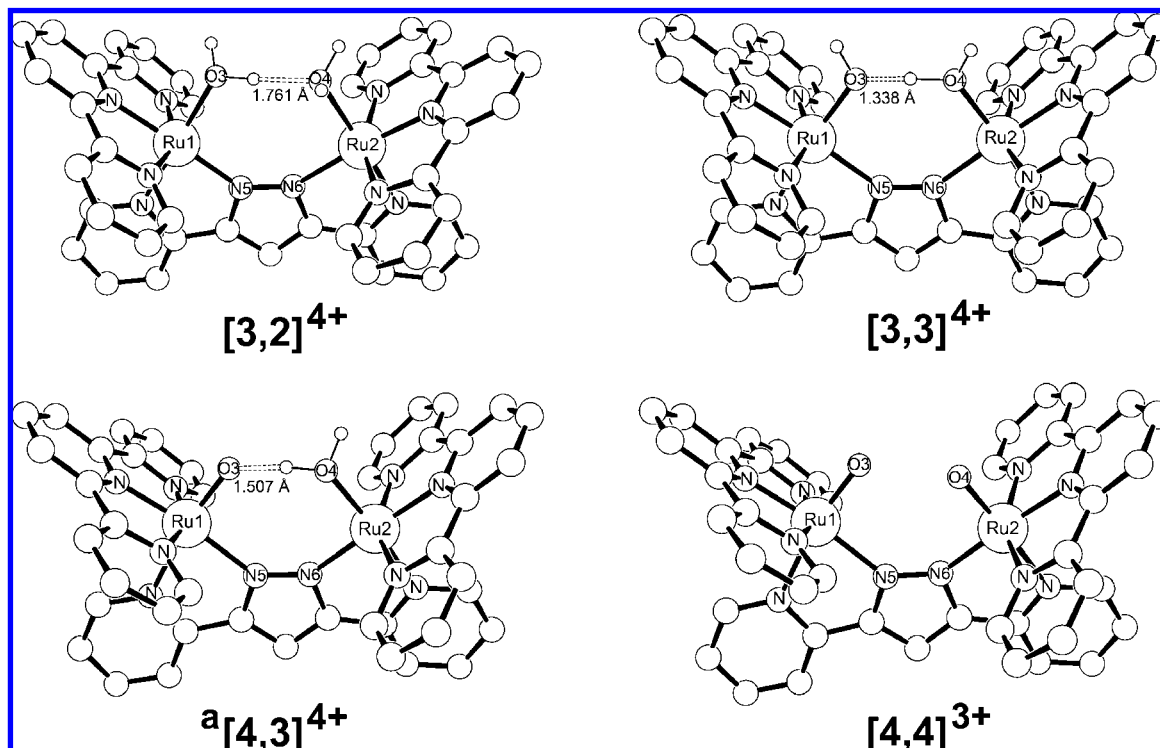(62) Salomon, O.; Reiher, M.; Hess, B. A. *J. Chem. Phys.* **2002**, *117*, 4729–4737.

Figure 2. Optimized structures of **[3,2]⁴⁺**, **[3,3]⁴⁺**, **ᵃ[4,3]⁴⁺**, and **[4,4]³⁺**.

Table 2. Selected Bond Lengths r (Å) and the O3−Ru1−Ru2−O4 torsional angle θ (deg) of the Most Relevant Redox Species

	[2,2]³⁺	[3,2]⁴⁺	[3,3]⁴⁺	ᵃ[4,3]⁴⁺	[4,4]³⁺
r(Ru1−O3)	2.309	2.189	2.068	1.794	1.783
r(Ru2−O4)	2.227	2.300	1.999	2.124	1.783
r(Ru1−N5)	2.182	2.074	2.146	2.200	2.145
r(Ru2−N6)	2.180	2.254	2.195	2.134	2.145
θ(O3−Ru1−Ru2−O4)	44.0	15.1	3.4	22.3	64.4

Table 3. Mulliken Spin Densities

	Mulliken spin density			
	Ru1	Ru2	O3	O4
[2,2]³⁺	0.0	0.0	0.0	0.0
[3,2]⁴⁺	0.7	0.0	0.0	0.0
[3,3]⁴⁺	0.8	−0.8	0.0	−0.1
ᵃ[4,3]⁴⁺	1.1	−0.8	0.8	0.0
[4,4]³⁺	0.9	−0.9	1.0	−1.0

Table 4. Relative Free Energies for Various Spin States of **[3,3]** and **[4,4]** Ions (Referenced to AF)ᵃ

	[3,3]⁴⁺	[3,3]³⁺	[3,3]²⁺	[4,4]⁴⁺	[4,4]³⁺
AF	0.0	0.0	0.0	0.0	0.0
S	27.70	24.33	9.24	28.01	44.84
T	0.80	0.44	−2.88	8.91	7.24
Q	N/A	N/A	N/A	3.15	−0.77

ᵃ AF, antiferromagnetic state; T, triplet state; Q, quintet state; S, symmetric singlet state.

since $E°[\text{Ce(IV)/Ce(III)}] = 1.70$ V vs. NHE in HClO₄.[63] Thus, our calculations support Llobet's proposal that **[4,4]³⁺** is the catalytically active species.

Mechanistic Exploration. Beyond the removal of four electrons and four protons, formation of free dioxygen is indispen-

(63) Connelly, N. G.; Geiger, W. E. *Chem. Rev.* **1996**, *96*, 877–910.

Table 5. Calculated and Experimental Redox Potentials (V) at pH 1ᵃ

	$E_{1/2}$(calcd)	$E_{1/2}$(calcd)$_{pH1}$	$E_{1/2}$(exptl)	difference
[3,2]⁴⁺ + e⁻ → [2,2]³⁺	0.598	0.598	0.520	0.078
[3,3]⁴⁺ + e⁻ + H⁺ → [3,2]⁴⁺	0.515	0.456	0.600	−0.144
ᵃ[4,3]⁴⁺ + e⁻ + H⁺ → [3,3]⁴⁺	1.075	1.016	0.840	0.176
[4,3]⁴⁺ + e⁻ + H⁺ → [3,3]⁴⁺	1.569	1.510	0.840	0.670
[4,4]³⁺ + e⁻ + 2H⁺ → ᵃ[4,3]⁴⁺	1.472	1.354	1.05	0.304
[5,4]⁴⁺ + e⁻ → [4,4]³⁺	1.875*	1.875*	N/A	N/A
[5,5]⁵⁺ + 2e⁻ → [4,4]³⁺	2.032*	2.032*	N/A	N/A

ᵃ Potentials from ref 11 are referenced to SSCE, and the computed potentials are referenced accordingly. Values marked with * are referenced to NHE.

Scheme 5
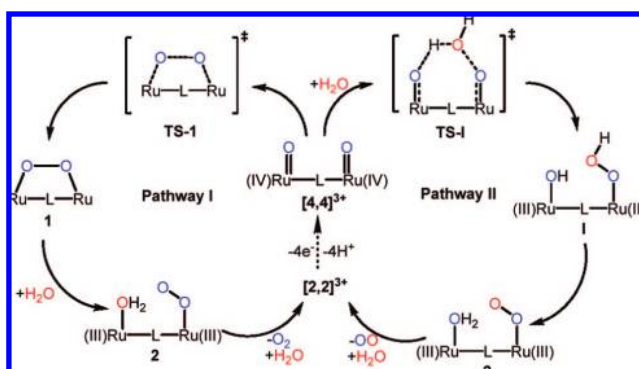
sible in the water oxidation reaction. Of the many speculations on the key O−O bond formation process, the two most attractive scenarios are outlined in Scheme 3. Since no isotope-labeling experiment to distinguish the two mechanisms has been reported to date, it is necessary to carefully examine both reaction pathways, which are outlined in more detail in Scheme 5. In reaction pathway I, **[4,4]³⁺** undergoes direct oxo−oxo coupling
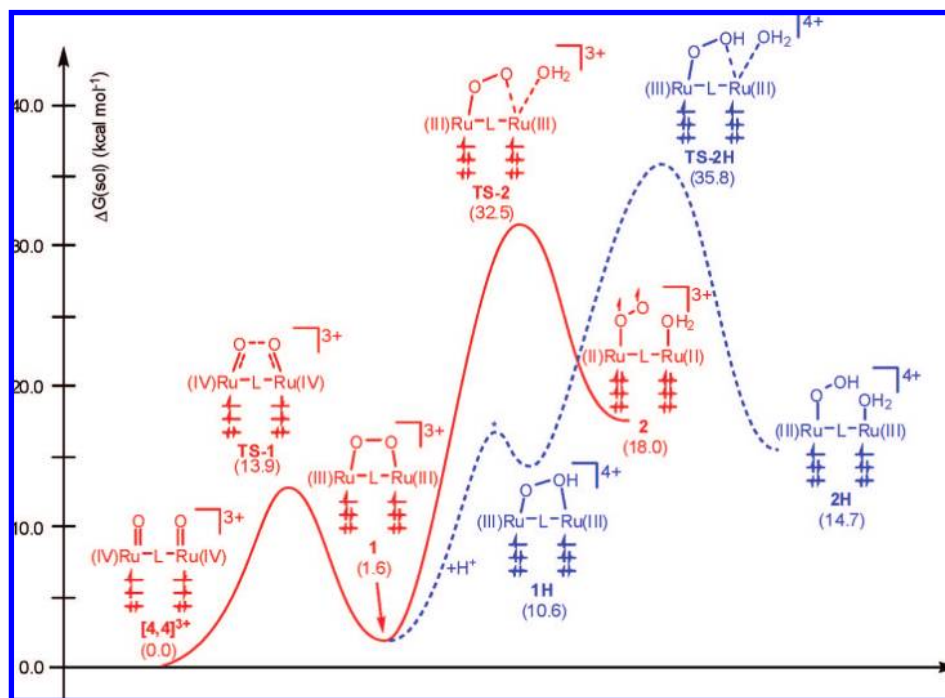
Figure 3. Reaction energy profile for direct oxo−oxo coupling to form the O−O single bond and the subsequent processes (red solid line) and that showing the effect of acid catalysis on the water substitution reaction (blue dashed line).
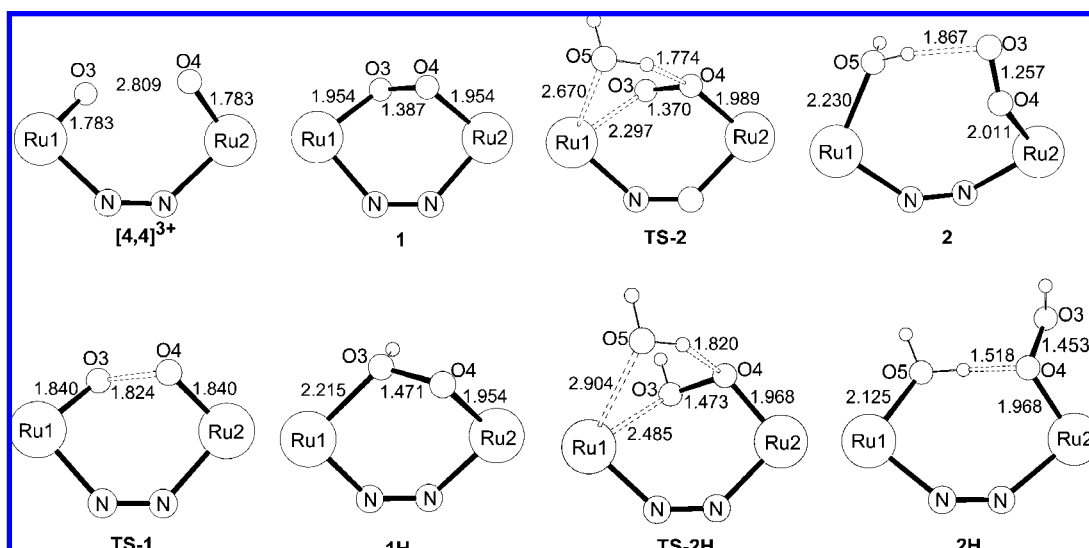

Figure 4. Optimized structures and selected bond lengths (Å) of species involved in Figure 3.

to yield a diruthenium peroxo intermediate, which is followed by water addition to complete the four-electron reduction of the catalyst and produce O_2. Reaction pathway II takes water addition across the two terminal oxo atoms as the first step, giving rise to a hydroxo/hydroperoxo diruthenium intermediate; this is followed by proton transfer and reductive elimination of O_2 to regenerate the procatalyst $[2,2]^{3+}$.

Reaction Pathway I: Direct Oxo−Oxo Coupling in $[4,4]^{3+}$. We anticipated that O−O bond formation in $[4,4]^{3+}$ would occur through the direct coupling of the two terminal oxo groups on the basis of the following reasoning: (1) Though the two terminal oxo atoms are separated by 2.089 Å, their relative position is tightly locked by the rigid bridging bipyridylpyrazolylic ligand in a facial manner, which should significantly reduce the energetic cost for structural reorganization during the intramo-

lecular oxo−oxo coupling process. In the blue dimer, the two terminal oxo atoms are positioned orthogonally, with a large separation of ∼5 Å. (2) The two radicaloid oxygen atoms with opposite spin orientations resulting from the antiferromagneti-cally coupled ground state should facilitate the O−O single-bond formation through diradical coupling. (3) Intramolecular coupling is entropically favored.

The reaction energy profiles for pathway I are shown in Figure 3, and the structures of the species involved are depicted in Figure 4. Traversing an unsurprisingly low transition state **TS-1** at 13.9 kcal mol^{-1}, the direct intramolecular oxo−oxo coupling affords intermediate **1**, which is nearly isoenergetic to its precursor $[4,4]^{3+}$. Since the antiferromagnetically coupled state of **1** has a negligibly lower free energy than the triplet state ($\Delta G = 0.2$ kcal mol^{-1}) and the subsequent intermediates/

Table 6. Mulliken Spin Densities for Species Involved in Figure 3

	Ru1	Ru2	O3	O4	O5
$[4,4]^{3+}$	0.9	−0.9	1.0	−1.0	N/A
TS-1	0.7	−0.7	0.7	−0.7	N/A
1	0.6	0.6	0.3	0.3	N/A
TS-2	0.6	0.5	0.4	0.3	0.0
2	0.0	0.4	0.8	0.7	0.0
1H	0.8	0.8	0.0	0.2	N/A
TS-2H	0.8	0.8	0.0	0.2	0.0
2H	0.8	0.8	0.0	0.2	0.0

transition states have either triplet ground states or negligible energy differences between the AF and T states ($\Delta G < 0.5$ kcal/mol), we propose an intersystem spin crossing from the overall singlet state to the triplet state of **1** for convenient O₂ production later. In our previous work,[30] Mulliken spin density analysis was established as a reliable tool for tracking changes in metal oxidation states, thus tracing the electron flow from the substrate to the catalyst. As the spin densities shown in Table 6 indicate, both ruthenium centers of intermediate **1** are at oxidation states of +3, and the bridging group is formally assigned to be a peroxo group. Thus, two electrons are successfully transferred to the ruthenium centers from the terminal oxo atoms upon formation of **1** from the reactant species.

In an effort to regenerate the catalyst, the bridging peroxo group has to be further oxidized to form O₂ gas, which can diffuse away from the bimetallic core. There are several possibilities for achieving that goal: (1) Direct reductive elimination of O₂ without water participation via a dissociative mechanism passes the remaining two electrons to the two ruthenium centers in a concerted fashion. This one-step mechanism, however, may not be practical because of the formation of thermodynamically unfavorable five-coordinate Ru(II) centers. (2) Two water molecules participate simultaneously in the reductive elimination process to avoid the coordinatively unsaturated intermediate. Consequently, we anticipate a high-energy transition state because of the large entropy penalty to be expected for such a three-body transition state. (3) Combining the advantages of the above two options, we analyzed in detail a mechanism in which the bridging peroxo group is replaced by two water molecules in a stepwise fashion. A high barrier (30.9 kcal mol⁻¹) is obtained at **TS-2** when the first substitution reaction takes place (Figure 3). The resulting intermediate **2** is terminated by an aqua ligand and an O–O ligand that has spin properties resembling that of free molecular dioxygen, and both ruthenium centers are at an oxidation state of +2. Observing the overall reaction barrier measured between $[4,4]^{3+}$ and **TS-2** to be as high as 32.5 kcal mol⁻¹, we conclude that reaction pathway I via direct intramolecuar oxo–oxo coupling is unproductive toward the overall water oxidation reaction under the given experimental condition, i.e., room temperature.

Considering that the neutral water molecule is a much weaker nucleophile than the dianionic peroxo ligand, we reasoned that the acidic medium may provide a potential solution to the above-described mechanistic dilemma. Protonation of the bridging peroxo ligand should weaken one of the Ru–O bonds, thus yielding more space for the approaching water molecules and facilitating the associative substitution reaction. As anticipated, the Ru1–O3 bond length is significantly elongated by 0.261 Å (Figure 4), and no significant change in the spin densities of the key atoms is observed when O3 is protonated (Table 6). Though the reaction barrier for the water substitution (**1H** → **TS-2H**) is 5.2 kcal mol⁻¹ less than that in the previous

unprotonated situation (**1** → **TS-2**), the overall barrier increases by 3.8 kcal mol⁻¹ as a result of the large energy penalty (9.0 kcal mol⁻¹) for forming the protonated state **1H** from **1**. Thus, neither of the above-described mechanistic scenarios involving the facile intramolecular oxo–oxo coupling process is productive toward O₂ formation, because of the high barrier in the water substitution reaction to form the aqua/O–O intermediate **2** or its protonated analogue **2H**, which are key precursors of the O₂ production and catalyst-regeneration steps.

Reaction Pathway II: Coupling between Terminal Oxo and Water Oxygen Atoms. Reaction pathway II (Scheme 5) regained our attention after we concluded that the facile oxo–oxo coupling is unproductive in the end. Convincing experimental evidence[33,64] from the blue dimer studies supports O–O bond formation via reaction pathway II for that catalyst, and our previous calculations revealed that this key process occurs via a radical recombination mechanism, where the two terminal radicaloid oxo atoms having spin densities of opposite signs promote the homolytic splitting of one O–H bond in water to form the desired O–O bond. In view of the similar chemical property of the terminal Ru=O groups in the two systems, i.e., radicaloid terminal oxo atoms with opposite spin orientations, is it possible for $[4,4]^{3+}$ to replicate the same mechanism as observed for the blue dimer in the O–O bond formation process? When we followed the same scheme that we used for the blue dimer system, the transition-state searches on the AF state inevitably converged to the same structure having a relative free energy of 47.7 kcal mol⁻¹ (**TS-I$_{AF}$** in Figures 5 and 6), despite exhaustive efforts to find a lower-energy transition state. Surprisingly, negligible spin density was found on the ruthenium atom (Ru2) linked to the O–O bond being formed (Table 7), which indicates that Ru2 is in an oxidation state of +2. Therefore, the terminal oxo atom (O3) has already been oxidized by two electrons, yielding an empty orbital to accommodate the nucleophilic lone pair of the incoming water molecule. The O–H single bond of water is cleaved heterolytically, and the O–O bond forms via a Lewis acid/base type of interaction (Scheme 6a) rather than the homolysis performed by the active form of the blue dimer reported previously. The unpaired-electron spin densities (0.9) on the ruthenium atoms of $[4,4]^{3+}$ were found to be 40% less than those in the active form of the blue dimer (1.5), which indicates that Ru(IV) does not have enough oxidizing potential to generate the sufficiently powerful radicaloid oxygen radical that is required by the radical recombination process at the transition state. The Lewis acid/base-type O–O bond formation indicated by our calculations, however, leads to another extreme with a higher energy input that requires only one Ru(IV) to completely withdraw as many as two electrons from the terminal oxo atom in a single step, while the other Ru(IV) behaves as an innocent observer. A similar O–O bond formation mechanism is found at the corresponding triplet transition state (**TS-I$_T$** in Figure 5), with insignificant structural variations (Figure 6) but a barrier that is lower by 7.5 kcal mol⁻¹. We rationalize the lower barrier on the triplet surface in terms of a smaller internal electron-reorganization penalty (Scheme 6b) as opposed to the significant rearrangement from the open-shell singlet at $[4,4]^{3+}$ to the closed-shell singlet at the transition state **TS-1$_{AF}$** (Scheme 6a). This observation is even more remarkable in view of the spin-state transition between the AF and T states, which is 7.2 kcal mol⁻¹ in the opposite direction. Therefore, our mechanistic

(64) Geselowitz, D.; Meyer, T. J. *Inorg. Chem.* **1990**, *29*, 3894–3896.
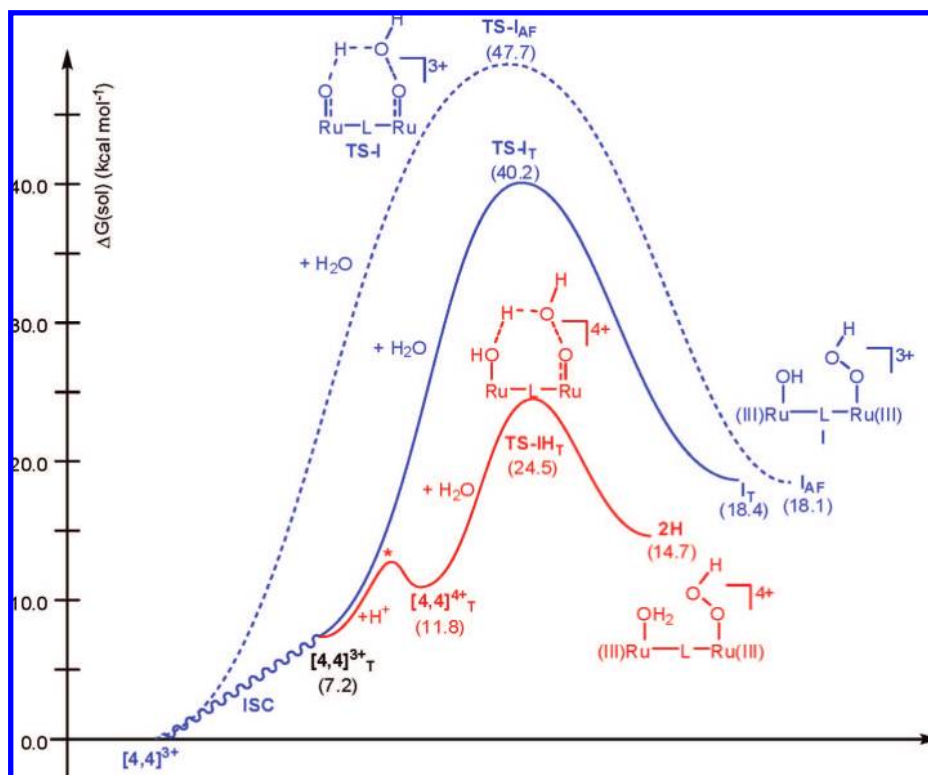
Figure 5. Reaction pathway II: Energy profiles in blue show the coupling between terminal oxo and water oxygen atoms during O−O bond formation (dashed line, AF state; solid line, T state); The red line shows the proton-catalyzed process. ISC means intersystem spin crossing.
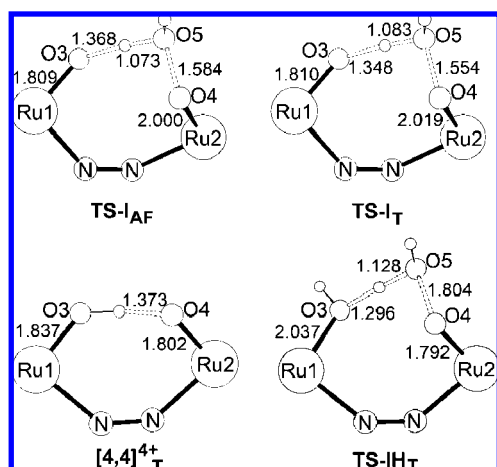

Figure 6. Structures and bond lengths (Å) of selected intermediates and transition states in Figure 5 and Scheme 6.

Table 7. Mulliken Spin Densities for Species Involved in Figure 5

	Ru1	Ru2	O3	O4	O5
$[4,4]^{3+}{}_T$	0.9	0.0	1.0	0.0	N/A
$[4,4]^{4+}{}_T$	1.3	−0.1	0.6	0.1	N/A
TS-I$_{AF}$	0.1	0.0	−0.2	0.0	0.0
TS-I$_T$	1.1	0.1	0.7	0.0	0.0
TS-IH$_T$	0.9	0.8	0.1	0.3	0.2

discussion below is confined to the triplet surface for all of the intermediates and transition states after $[4,4]^{3+}$.

In order to rationally improve the performance of the catalyst, two Ru(IV) centers must work cooperatively in the water splitting process. A wishful solution is shown in Scheme 7. Is it possible to disproportionate Ru(IV)−L−Ru(IV) to Ru(III)−

Scheme 6
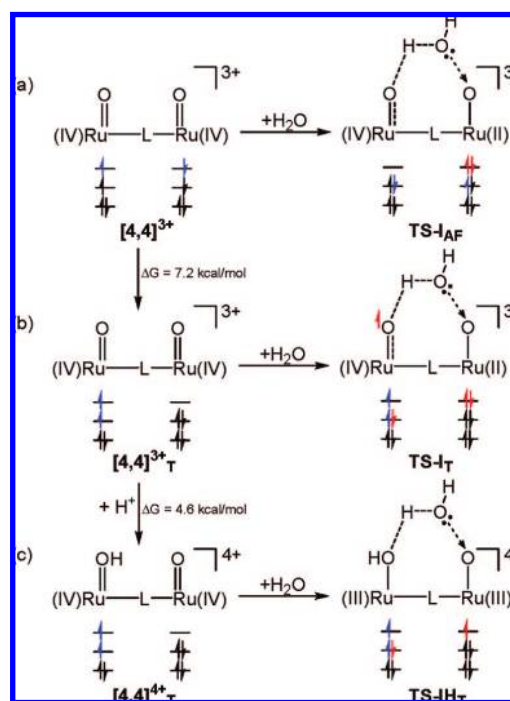
L−Ru(V), thereby generating a more powerful oxidizing center Ru(V) to carry the Lewis acid/base-type O−O bond formation mechanism discovered above? An intuitive and straightforward thought is to introduce an additional proton on one of the terminal oxo atoms, thus breaking the pseudo-C_2 symmetry of the molecule and providing different chemical environments around the two ruthenium centers. In principle, the ruthenium with the electrostatically weaker monoanionic hydroxo ligand

Scheme 7
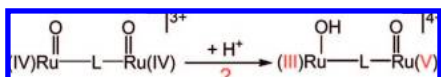
should attract more electron density and become less oxidizing than the unperturbed Ru(IV). Only a very small amount of energy (4.6 kcal mol^{-1}) is required to protonate $[4,4]^{3+}_T$. The spin densities on the two ruthenium centers of $[4,4]^{3+}_T$ are shifted as anticipated after protonation, though not to a significant extent (Table 7). On the basis of the Mulliken spin densities, the protonated state still has both ruthenium atoms at an oxidation state of +4, denoted $[4,4]^{4+}_T$. Drastic change occurs, however, at the transition state ($\mathbf{TS\text{-}IH_T}$) where the two ruthenium centers display the characteristic spin densities of the +3 oxidation state (0.9 and 0.8 respectively) and near-zero spin density exists on the approaching water oxygen. Remarkably, the activation barrier is lowered dramatically from the original 40.2 to 24.5 kcal mol^{-1}, which is comparable to the reaction barrier found in the blue dimer study (25.6 kcal mol^{-1}) and consistent with the experimental observation that this reaction goes to completion at room temperature.

What does that magic proton do at the transition state **TS-IH$_T$**? On the basis of a careful comparison of the electron densities of **TS-I** and **TS-IH$_T$**, the answer is summarized in Scheme 6b,c. Protonation of the terminal oxo group (O1) at **TS-IH$_T$** effectively stops the intrinsic flow of electron density to its neighboring electron-deficient Ru(IV) center (Ru1), which instead withdraws electron density from the other metal site (Ru2). Thus, the proton helps to direct the oxidative power of the Ru1 center toward Ru2, where the actual oxidation of the incoming water substrate takes place. With the combined oxidizing power of both ruthenium centers, there is enough oxidation potential to formally remove two electrons from the terminal oxo atom (O4), which can then act as the Lewis acid that attacks the oxygen of the incoming water to engage in a facile O–O bond formation process.

Summary of the Proposed Mechanism. Our proposed mechanism is summarized in Figure 7. First, the resting state of the catalyst $[4,4]^{3+}$ undergoes spin crossover to its triplet state $[4,4]^{3+}_T$, which is followed by protonation of one of the terminal oxo groups to avoid the high-energy transition state **TS-I**. To rationalize the key reactivity and understand the features of the catalyst that lead to the remarkable oxidative cleavage of the O–H bond of water, it is helpful to consider the disproportionated resonance form of $[4,4]^{4+}_T$, denoted $[3,5]^{4+}$. It should be noted that we are not proposing the existence of such a species but instead are visualizing electronic distortions that are consistent with the electronic features we found at the transition state. Our analysis shows that one plausible explanation of the reactivity is the *in situ* formation of a powerful Ru(V) center that evacuates two electrons from the terminal oxo moiety, which in turn can act as a powerful Lewis acid and engage in a heterolytic O–O bond formation event with the incoming water, traversing the transition state **TS-IH$_T$**. This step is rate-determining, with an activation barrier of 24.5 kcal mol^{-1}, and gives the aqua/hydroperoxo intermediate **2H**, in good agreement with the experimental observation that this reaction is viable under ambient conditions. The endgame of the catalytic cycle includes a slightly endergonic deprotonation to give intermediate **2**. We propose two fictitious intermediates, **2*** and **2****, to rationalize the complicated spin-density changes that afford complex **2** from **2H**. As **2H** loses the proton, the anionic

hydroperoxo ligand becomes an electrostatically much stronger dianionic ligand. This creates an energy gradient in **2*** for intramolecular electron transfer as a result of the different electrostatic field strengths generated by the aqua and peroxo ligands on the two ruthenium centers. Consequently, a disproportionation occurs to give a (H$_2$O)–Ru(II)–L–Ru(IV)–(OO) core, the conceptual species **2****. The newly formed Ru(IV) center can engage in a two-electron oxidation of the peroxo ligand to form intermediate **2**, which we were able to locate as a stable intermediate. Although the O$_2$ unit is still attached to the Ru center, its electronic structure is essentially that of free dioxygen in this complex. Facile O$_2$ dissociation from this complex is expected, with a second water molecule taking its place to regenerate the procatalyst $[2,2]^{3+}$.

Redox Stability of the Key Intermediates. To this point, we have proposed a Lewis acid/base-type mechanism for the water splitting reaction and subsequent reaction path leading to free O$_2$ production. One issue out of many that may affect the validity of the above model is the redox stability of the many intermediates we have examined in the two reaction pathways. A particularly important one is species **1**. Since it is nearly isoenergetic to $[4,4]^{3+}$, **1** may have a sufficiently long lifetime to be oxidized by Ce(IV), unlike the other transient intermediates **2** and **2H** that are likely be short-lived. In any case, if these intermediates undergo oxidation, they may give rise to more complicated reaction pathways than the one outlined above. Table 8 summarizes the redox potentials we have computed to be required for oxidation of the three most important intermediates: **1**, **2** and **2H**. We have tabulated the reduction potentials of the oxidized species in accord with normal convention of listing redox potentials. At a normal redox potential of 1.837 V, Ce(IV) is not powerful enough to oxidize **1** by one electron, thus eliminating any redox-triggered alternative pathway from intermediate **1** and supporting our conclusion that pathway I is meaningless and invalid. The only intermediate that may be affected is intermediate **2**, which has a redox potential of only 1.023 V and may be oxidized to give **2$^+$** if the oxidation is kinetically more facile than dioxygen release. In principle, **2$^+$** should facilitate more rapid reductive elimination of O$_2$ as a result of removal of one electron from the metal centers. Similar to Meyer's earlier work on global kinetic measurements for the blue dimer,[65] more detailed experimental work on the kinetics of the present system would be helpful in delineating the details of the mechanism. In any case, these processes would likely occur after the rate-determining step and thus be less important for understanding the main driving force for the water oxidation process. They may, however, play a critical role in side reactions that may lead to undesired products and catalyst deactivation.

Conclusions

In conclusion, we have carefully examined the structures and redox properties of the most important intermediates from $[2,2]^{3+}$ to $[4,4]^{3+}$. Among the most abundant redox intermediates, antiferromagnetically coupled states are found to be the ground states when possible, e.g., for $[3,3]^{4+}$ and $[4,4]^{3+}$. An intramolecular hydrogen bonding persists throughout the entire series except in $[4,4]^{3+}$, which displays two radicaloid terminal oxygen atoms with opposite spin orientations. An unusual structure is found at the [4,3] oxidation level with a total charge of +4. This redox species, denoted $^a[4,3]^{4+}$, displays an

(65) Chronister, C. W.; Binstead, R. A.; Ni, J. F.; Meyer, T. J. *Inorg. Chem.* **1997**, *36*, 3814–3815.
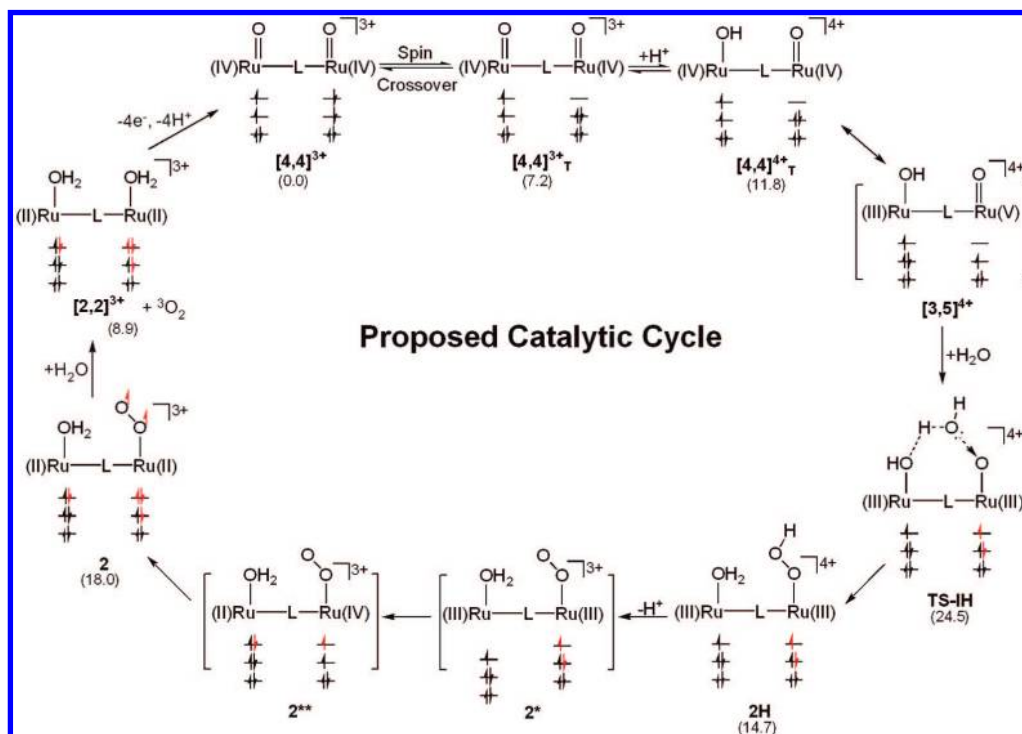
Figure 7. Summary of a plausible mechanism for water oxidation catalysis proposed in this work. The most important four electrons originating from oxygen atoms are colored in red.

Table 8. Calculated Single-Electron Redox Potentials vs. NHE of **1**, **2**, and **2H**

	$E_{1/2}$ (V)
$1^+ + e^- \rightarrow 1$	1.837
$2^+ + e^- \rightarrow 2$	1.023
$2H^+ + e^- \rightarrow 2H$	2.031

asymmetric proton distribution on the two terminal sites (i.e., Ru(IV)=O vs Ru(III)−OH₂). A plausible explanation of the formation of ᵃ[4,3]⁴⁺, based on the weak coupling nature of its redox precursor [3,3]⁴⁺, is provided. Our computed redox potentials are in good agreement with experimental values for the first three reversible redox processes, whereas a slightly larger deviation is found for the fourth irreversible one. We were able to provide evidence in support of [4,4]³⁺ being the active catalyst. The possible complexes of higher oxidation states, such as [5,4]⁴⁺ and [5,5]⁵⁺, are associated with prohibitive oxidation potentials. Two possible reaction pathways starting from [4,4]³⁺ were carefully examined in this work: intramolecular oxo−oxo coupling (reaction pathway I) and coupling between water oxygen and terminal oxo atoms (reaction pathway II). As anticipated, a facile intramolecular oxo−oxo coupling is found, with a barrier of 13.9 kcal mol⁻¹. The following substitution of the peroxo group to afford the peroxo/aqua intermediate **2**, however, is prohibitively high in energy, with a barrier of 32.5 kcal mol⁻¹. We concluded that the intramolecular oxo−oxo coupling is possible but unproductive toward dioxygen evolution. Pathway II is identified to be much more feasible and relevant. The key O−O bond is formed between a water substrate and one of the O=Ru moieties to afford a peroxo intermediate; this is the rate-determining step, with a barrier of 24.5 kcal mol⁻¹. Deprotonation and disproportionation of the two Ru(III) centers formally afford a Ru(IV)−(OO) system that

completes the catalytic cycle by removal of two electrons from the peroxo moiety to give molecular dioxygen. Whereas superficial similarities between this mechanism and that proposed for the blue dimer can readily be recognized, the critical details are radically different. First, the O−H bond of water is broken in a heterolytic fashion and the oxygen of the water substrate acts as a Lewis base. In contrast, the blue dimer oxidizes water through a homolytic bond cleavage event involving a radicaloid Ru−oxo system. Second, a proton plays a pivotal role in stabilizing the transition state by nearly 16 kcal mol⁻¹, from 40.2 to 24.5 kcal mol⁻¹. The addition and removal of protons also played an important role in the blue dimer case, but protons did not play such a direct role for the O−H bond activation mechanism. This work highlights a second mechanistic scenario that can lead to water oxidation. Rather than a radical-recombination type of mechanism as was outlined in our previous work, we found a Lewis acid/base type of interaction being operative for the key oxygen−oxygen coupling reaction.

Supporting Information Available: Cartesian coordinates of all of the structures, vibrational frequencies, and all of the energy components. This material is available free of charge via the Internet at http://pubs.acs.org.

JA8034043